This item is the archived peer-reviewed author-version of:

Modeling a Langmuir probe in atmospheric pressure plasma at different EEDFs

Modelling a Langmuir probe in atmospheric pressure plasma at different EEDFs

G Trenchev[1], St Kolev[2], Zh Kiss'ovski[2]

[1]Research group PLASMANT, Department of Chemistry, University of Antwerp, Universiteitsplein 1, 2610 Antwerp, Belgium
[2]Faculty of Physics, Sofia University "St Kliment Ohridski", 5 James Bourchier Boulevard, 1164 Sofia, Bulgaria

E-Mail: georgi.trenchev@uantwerpen.be and skolev@phys.uni-sofia.bg

Abstract. In this study, we present a computational model of a cylindrical electric probe in atmospheric pressure argon plasma. The plasma properties are varied in terms of density and electron temperature. Furthermore, results for plasmas with Maxwellian and non-Maxwellian electron energy distribution functions are also obtained and compared. The model is based on the fluid description of plasma within the COMSOL software package. The results for the ion saturation current are compared and show good agreement with existing analytical Langmuir probe theories. A strong dependence between the ion saturation current and the electron transport properties was observed, and attributed to the effects of the ambipolar diffusion.

1. Introduction

The electric plasma probe (Langmuir probe) is a well-known diagnostics tool for a variety of low to high pressure thermal and non-thermal plasmas, because of its simple means and wide range of applicability. Over the last several decades, the Langmuir probe has been used extensively as a diagnostic tool for determining plasma parameters such as electron density, ion density, electron temperature and plasma potential.

The probe itself consists of a small electrode (usually a metal cylinder, a sphere, or a disk), typically biased in the range from -50 to +50 V with respect to a much larger reference electrode [1]. There are also double, triple, and multi-probe configurations specialized for a variety of conditions [2]. The data for the plasma parameters is extracted from the current-voltage characteristic of the probe by applying the appropriate theories and relations for the present conditions [3, 4]. Conditions can vary by a vast degree, for instance, plasmas can be in a low (10^{-9} to 10^{-3} bar), moderate (10^{-2} bar)

and high (1 atm. and above) pressure. The electron and ion temperatures determine whether the plasma is in thermal equilibrium ($T_e \approx T_i$) or is a low-temperature non-equilibrium plasma ($T_e > T_i$). Depending on the mean free path for the ions, plasmas can be also collisional or non-collisional, which will lead to different assumptions when analysing the plasma sheaths. Furthermore, plasmas can be subjected to gas flows or remain stationary. It is easy to see that the number of possible combinations is very large, and so is the number of plasma probe theories as well.

The progress on electric probes dates from 1926 with Mott-Smith and I. Langmuir's well-known work for low pressure plasmas [3]. Some very extensive literature on the subject is present [4]. A considerable progress has been made with analytical and numerical models for a variety of probe and plasma parameters at low, moderate and atmospheric pressure plasma. Low-pressure numerical models have been developed [5, 6]. Other works review probes in flowing plasma conditions at moderate to high pressures [7, 8]. A vast amount of experimental and theoretical works belong to the low-temperature plasmas [9-16]. Some recent investigations were conducted for probes in low-temperature, atmospheric microwave plasma [17, 18]. Plasmas employed in industry, medicine and scientific research typically fall into this category. While the electric probe is often employed in the experiments with plasma, and the theoretical background behind it is very extensive, challenges are still faced when combining different electric probe theories with the experimental data.

At atmospheric pressure, the mean free path of electrons and ions is usually smaller than the probe diameter, which results in a much stronger gradient of the plasma density near the probe. On the other hand, the probe should be as thin as possible (taking into account the limitations due to the thermal conductivity of the wire), or otherwise it will introduce various disturbances in the surrounding plasma, resulting in inaccurate measurements. The cylindrical shape of the probe also represents a difficulty in obtaining an analytical solution for the probe current [1, 11, 15]. A number of plasma probe theories have been developed in order to evaluate the plasma parameters (typically electron density and temperature) at atmospheric pressure.

Nowadays, the calculation speed of modern computers allows developing a reliable numerical model for the researcher to use in aid to the electric probe experiments. The goal of this work is to develop such a model, and benchmark one of the existing analytical Langmuir probe theories at atmospheric pressure against a more elaborate numerical model, including proper description of the sheath around the probe.

Section 2 of the paper describes the model in detail, including the system of equations, the reaction rate set and the boundary conditions.

Section 3 describes the analytical probe theory chosen to be benchmarked with the numerical model.

Section 4 is the result section, where the data for probe current-voltage characteristic obtained from the model is presented. The ion saturation current is taken under consideration under different plasma densities and electron temperatures.

The paper concludes with Section 5, where some additional remarks on the model performance are added to the discussion.

2. Model description

2.1 System of equations

The model is build using the Plasma module in Comsol Multiphysics [19]. This module offers the fluid description of plasma through its DC Discharge interface. Fluid plasma models are based on macroscopic quantities of particles like densities, mean velocity and mean energy for the plasma species (i.e. electrons, ions and excited species). Their computational cost is significantly reduced compared to kinetic models. The fluid model used here is based on a set of equations for the particle

densities, defined within the drift-diffusion approximation. Thus, the obtained results are only an approximate description of the plasma, which is justified by the complex nature of the task.

2.1.1 Particle balance equations

Under the drift-diffusion approximation, the following equation is solved for the particle balance of electrons, ions of different types, and excited atoms:

$$\frac{\partial n_s}{\partial t} + \nabla \cdot \overrightarrow{G_s} = S_c \tag{1}$$

where n_s stands for species density, $\overrightarrow{G_s}$ stands for species flux, and S_c is the production term, which represents the particles produced or lost due to volume reactions. The electron flux would be described as follows:

$$\overrightarrow{G_e} = -\nabla(D_e n_e) + \frac{q_e}{|q_e|} \mu_e n_e \vec{E} \tag{2}$$

where $\overrightarrow{G_e}$ stands for the electron flux, D_e and n_e stand for the electron diffusion and electron density respectively, q_e is the electron electrical charge, μ_e is the electron mobility, and $\vec{E}$ represents the electric field. Then, the ion flux is:

$$\overrightarrow{G_i} = -\nabla(D_i n_i) + \frac{q_i}{|q_i|} \mu_i n_i \vec{E} \tag{3}$$

where, by analogy, $\overrightarrow{G_i}$ stands for the ion flux, D_i stands for ion diffusion, and n_i for ion density. The use of the drift-diffusion approximation for the ions (eq. 3) is justified by the fact that for the considered conditions of atmospheric pressure plasma, the inertial term in the ion momentum balance equation remains several orders of magnitude smaller, compared to the other most significant terms. Finally, in the equation for the neutral species, the flux is determined only by diffusion:

$$\overrightarrow{G_s} = -\nabla(D_s n_s) \tag{4}$$

The electron mobility coefficient is derived from BOLSIG+ [20] and the Ar^+ mobility is defined as in [21]:

$$\mu_i = \frac{1.01 \times 10^5}{p_g (Pa)} \frac{T_g(K)}{273.16} 1.52 \times 10^{-4} \ (m^2 V^{-1} s^{-1}) \tag{5}$$

The electron diffusion coefficients is derived from the Einstein relation for plasmas with Maxwellian EEDFs. For non-Maxwellian distributions, the latter would not be correct (except if the electron-neutral collision frequency is assumed to be constant), and the diffusion coefficient is obtained directly from Bolsig+. The diffusion coefficient for $Ar(4s)$ is defined according to [22]:

$$D_{Ar(4s)} = \left(\frac{1}{n_{Ar}(m^{-3})}\right) 1.16 \times 10^{20} (T_{Ar}(K)/300)^{1/2} \ (m^2 s^{-1}) \tag{6}$$

The definition is the same for the diffusion coefficient of $Ar(4p)$. The temperature of all heavy species is assumed to be the same as the gas temperature T_g. In the above expression, n_{Ar} stands for the density of argon atoms.

2.1.2 Poisson equation

The balance equations are coupled with the Poisson equation for calculating the electric field in the model:

$$\Delta \varphi = -\frac{\rho}{\varepsilon_0}$$

(7)

where φ is the electric potential, ρ is the electric charge density and ε_0 is the dielectric permittivity of free space.

2.2 Plasma kinetics

Argon gas is considered in the model, as this is one of the most often used gases in plasma technologies. The electron impact reactions, chemistry kinetics and surface impact reactions are reduced only to the most significant ones. The species, considered in the model are electrons (e), atomic ions (Ar$^+$), and two species, representing lumped excited states of the 4s and 4p blocks (Ar(4s), Ar(4p)). The argon atom density is assumed to be constant and it is derived from the ideal gas law based on the pressure (p$_{Ar}$) and the gas temperature (T$_g$), i.e. low ionization degree is assumed. Electron-to-electron collisions are not considered in the model. The electron impact processes are given in table 1, the heavy species processes are summarized in table 2.

Table 1. Electron collisions processes included in the model.

Reaction	Rate coefficient	Reference
(R1) $e + Ar \rightarrow e + Ar$	BS	[23]
(R2) $e + Ar \rightarrow e + Ar(4s)$	BS, LP	[23]
(R3) $e + Ar \rightarrow e + Ar(4p)$	BS, LP	[23]
(R4) $e + Ar \rightarrow e + e + Ar^+$	BS, LP	[23]
(R5) $e + Ar(4s) \rightarrow e + Ar(4p)$	BS	[24]
(R6) $e + Ar(4s) \rightarrow e + e + Ar^+$	BS	[25]
(R7) $e + Ar(4p) \rightarrow e + e + Ar^+$	BS	[25]
(R8) $e + Ar(4s) \rightarrow e + Ar$	BS	[23]
(R9) $e + Ar(4p) \rightarrow e + Ar$	BS	[23]
(R10) $e + Ar(4p) \rightarrow e + Ar(4s)$	BS	[24]
(R11) $e + e + Ar^+ \rightarrow Ar + e$	$k_{(m^6/s)} = 8.75 \times 10^{-39} T_e^{-4.5} (eV)$	[26]
(R12) $Ar^+ + e + Ar \rightarrow Ar + Ar$	$k_{(m^6/s)} = 1.5 \times 10^{-40} \left(T_g(K)/300\right)^{-2.5}$	[27]

BS: Boltzmann solver. The rate coefficients are calculated from the corresponding cross sections, based on solution of the Boltzmann equation with Bolsig+ [20].
LP – limited production. The collision rate "r" is calculated using constant (n_{ec}) electron density (i.e. $r = k n_{ec} n_{Ar}$) instead of (i.e. $r = k n_e n_{Ar}$), where n_{ec} is a constant parameter and n_{Ar} is the density of the argon atoms.

In addition to the reactions within the plasma volume, certain surface reactions need to be implemented in the model. When an excited particle hits a boundary, it will revert to its ground state, while the ions will be neutralized and also converted to atoms. These reactions are presented in Table 3. The sticking coefficient value of these reactions are usually considered to be close to 1 and it were assumed in the model to be exactly equal to 1 in the boundary condition expressions in Table 5. The boundary area to which they apply, are the surrounding ground electrode and the probe surface.

Table 2. Heavy species collisions and radiative transitions included in the model.

Reaction	Rate coefficient	Reference
(R13) $Ar(4s) + Ar(4s) \rightarrow e + Ar + Ar^+$	$k_{(m^3/s)} = 1.62 \times 10^{-16} \left(T_g(K)/300 \right)^{1/2}$	[28]
(R14) $Ar(4p) \rightarrow Ar(4s)$	$k_{(1/s)} = 4.4 \times 10^7$	[28]
(R15) $Ar(4s) \rightarrow Ar$	$g_{eff} \times \pi \times 10^8$	[28]
(R16) $Ar(4s) + Ar(4p) \rightarrow e + Ar^+ + Ar$	$k_{(m^3/s)} = 1.62 \times 10^{-16} \left(T_g(K)/300 \right)^{1/2}$	[28]
(R17) $Ar(4p) + Ar(4p) \rightarrow e + Ar^+ + Ar$	$k_{(m^3/s)} = 1.62 \times 10^{-16} \left(T_g(K)/300 \right)^{1/2}$	[28]
(R18) $Ar(4p) + Ar \rightarrow Ar(4s) + Ar$	$k_{(m^3/s)} = 5 \times 10^{-18}$	[29]

g_{eff} = characteristic unit [30]

Table 3. Surface impact reactions assumed in the model.

Reaction	Sticking coefficient
(R19) $Ar^+ \rightarrow Ar$	1
(R20) $Ar(4s) \rightarrow Ar$	1
(R21) $Ar(4p) \rightarrow Ar$	1

Surface reactions: Reactions at model boundaries – plasma walls and plasma probe.

As probably noted by the reader, the electron energy balance equation is missing in the list of equations used in the model. While we can include it without much efforts, its use will limit our study to a value of the electron temperature, obtained from the solution. Since our aim is to derive the probe current-voltage characteristics at various conditions, we intentionally drop the electron balance equation and set T_e as an external parameter in the range of interest between 1 and 3 eV. Imposing T_e means that the model is not self-consistent and we cannot close properly the system of equations. If we consider all the reactions in tables 1 and 2 and setting, T_e will lead to lack of steady state solution - the density will either rises enormously or the plasma will vanish and the density will go to zero. In order to stabilize the model, and to allow the derivation of steady state solution, the production of species is controlled (limited) by controlling the ionization processes and the production of excited species contributing by stepwise ionization. This is done by modifying the collision rates ("r") of these processes by using constant electron density (n_{ec}) for their calculation ($r = k n_{ec} n_{Ar}$), instead of the electron density variable itself ($r = k n_e n_{Ar}$). Note also that a constant value is added to the direct ionization process (R4), in order to have charged particle production even at low electron temperature, where the ionization rate coefficient calculated with Bolsig+ is very small.

Another important characteristic of the used model is the lack of molecular ions in the argon chemistry. Often, at intermediate and high pressure discharges, the molecular ions are significant in number and play an important role mainly due to the recombination process. In this work, the molecular ions were intentionally excluded, in order to allow a more consistent comparison with the analytical expressions. Preliminary results show that indeed the molecular ions change significantly the obtained probe characteristic and one should take that in mind, depending on the discharge conditions.

We would like to stress that not all reactions from the considered set are important for the considered conditions and certainly some of them could be removed. However we keep all of them in order to preserve the generality of the model and its validity in a wider range of discharge conditions (electron density, gas temperature, electron temperature, pressure, etc.). Thus this model should not be considered as an example of chemistry needed for proper description of the considered conditions but only as a source of proper results for the given conditions, despite the fact that some reactions and species might be unnecessary (redundant).

## 2.3. Electron energy distribution function (EEDF)

The model is computed for 2 different electron energy distribution functions (EEDFs). One is a classical Maxwellian distribution, and the other is a non-Maxwellian – the one computed with the Boltzmann solver Bolsig+ [20]. These distributions are given in the figure 1. The non-Maxwellian electron energy distributions derived from Bolsig+ have a different shape for the different averaged energy values, derived assuming a different electric field. The gas temperature is assumed to be 1600K, in accordance to experiments in [17]. The value is approximate and in general it may vary considerably among the different experiments and setups. However, usually atmospheric pressure discharges tend to produce considerable gas heating except in non-stationary/pulsed discharge like DBD or gliding arc. Therefore this value is considered by us to be in the "typical" range of gas temperature values, without claiming completeness.
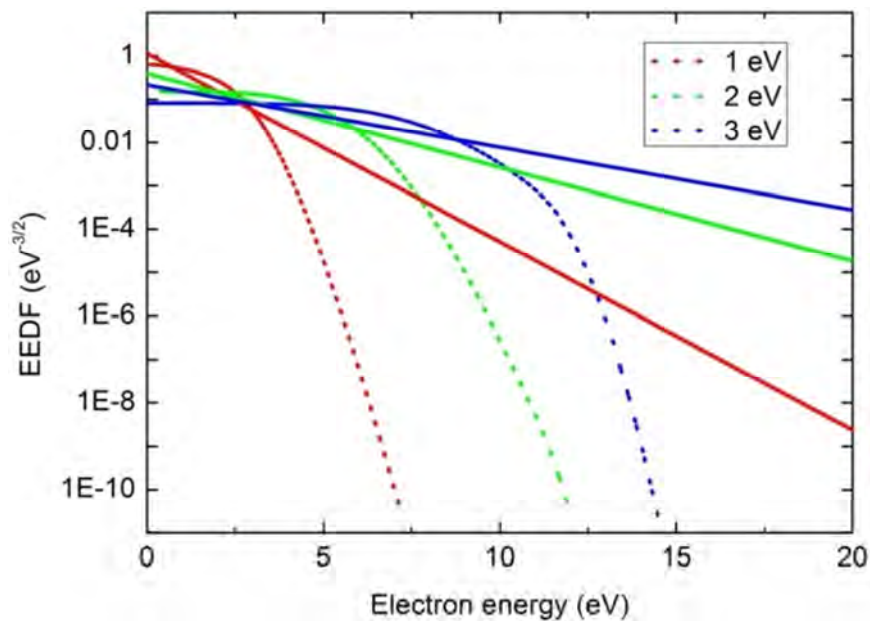

Figure 1. Electron energy, Maxwellian and non-Maxwellian distributions at $T_g = 1600K$. The non-Maxwellian EEDFs (dotted lines) are obtained with Bolsig+ and have the same averaged energy (or T_e) as the Maxwellian EEDFs (1, 2 and 3 eV). Mean electron energy in eV.

2.4 Model geometry and boundary conditions

The problem we consider is a cylindrical probe with length of 1 mm and radius of 0.05 mm, and both ends rounded with hemispheres. The plasma region is closed in a sphere with radius 10 mm and it plays the role of a reference electrode and it is grounded. In order to reduce the computational time, we take advantage of the symmetries, present in the problem – axial symmetry and symmetry with respect to the plane crossing the probe in the middle. As a result, the simulation domain reduces to the one presented at figures 2 and 3. In figure 3, the "insulation" boundary condition means zero fluxes of the charged particles and zero gradient of the electric field. As expected, the model requires a very fine finite element size at plasma sheath areas, typically in the order of 2 μm and smaller. Also, boundary mesh layers surround the electrode surfaces, with sizes down to 20 nm in direction perpendicular to the probe surface (see figure 2). The total number of mesh elements exceeds 50,000.
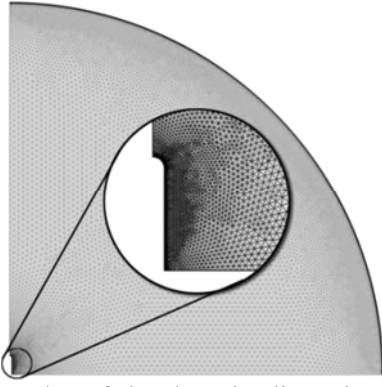
Figure 2. Plot of the domain discretization used in the model. Finite element size of less than 2 μm near the plasma probe surface is required.
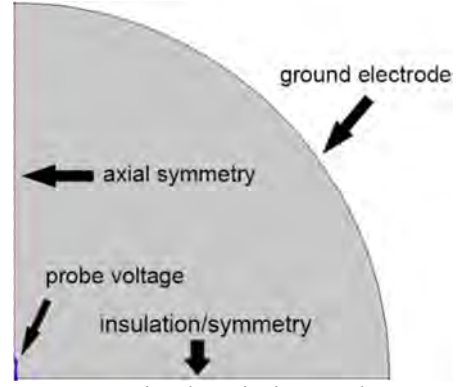
Figure 3. Domain description and some of the boundary conditions.

The bias voltage is applied at the probe boundary. The voltage slowly increases through a time-dependant function. The whole I-V characteristic is derived for time period of 20 s, which is large enough so that we can assume that at every point of the I-V characteristic, the plasma has reached a steady state. The outer boundary of the sphere is set at zero potential, as a ground electrode. Table 5 includes all boundary conditions used in the model. The probe current is evaluated at each time step taken by the solver by integrating current density over the probe surface. The final result is a current-voltage characteristic for the given conditions. The main model parameters are described in Table 4.

Table 4. Model parameters

Entity	Value	Unit
Probe length	1	mm
Probe radius	0.05	mm
Plasma density	$10^{17} \sim 10^{22}$	$1/m^3$
Electron temperature	$1 \sim 3$	eV
Pressure	1	atm
Probe bias	-50 ~ +50	V
Ion and gas temperature	1600	K

The boundary conditions (Table 5) for the model are taken from [30], with the according numbers for the expressions given below. Using the same modelling techniques, these expressions set the electrostatic conditions for the probe and wall entities in the model. The boundary conditions governing electron and field emission from [30] are not active in the present model.

Table 5. Boundary conditions

Boundary	Expression	Equation	Description
Probe	$\varphi = \varphi_0$	7	Voltage
Ground electrode	$\varphi = 0$	7	Voltage
Probe/Ground electrode	$\vec{n} \cdot \overrightarrow{G_i} = \frac{v_{i,th} n_i}{4} + \frac{q_i}{|q_i|} \mu_i n_i \vec{E} \cdot \vec{n}$	1 (n_i)	BC electrode
Probe/Ground electrode	$\vec{n} \cdot \overrightarrow{G_e} = \frac{v_{e,th} n_e}{2}$	1 (n_e)	BC electrode
Probe/Ground electrode	$\vec{n} \cdot \overrightarrow{G_s} = \frac{v_{s,th} n_s}{4}$	1 ($n_{Ar(4p)}, n_{Ar(4s)}$)	BC electrode
Axial symmetry	$\partial f / \partial r|_{r=0} = 0$	$1 - 7$	Axial symmetry
Insulation	$\vec{n} \cdot \overrightarrow{G_s} = 0$	1	No flux
Insulation	$\vec{n} \cdot D = 0$	7	Zero el. field

$\vec{n}$ is the normal vector; in column "expression" the number in brackets gives the equation number in the corresponding reference given on the left. In the axial symmetry boundary condition the letter "f" represents the dependent variables in equations 1-7. $v_{e,th} = \sqrt{\frac{8k_B T_e}{\pi m_e}}$, $v_{i,th} = \sqrt{\frac{8k_B T_i}{\pi m_i}}$, "BC"- Boundary Condition.

3. Probe theory

The results from the numerical model are compared with the continuum analytical theory of electrostatic probes developed by Su and Kiel [13]. The theory is essentially analogous to the paper by Su and Lam based on spherical probes [9], but it is approximated for probes of cylindrical shapes. In this theory, an elongated spheroid of the type $\frac{x^2}{a^2} + \frac{y^2}{b^2} + \frac{z^2}{c^2} = 1$, where $c > a$ is considered as the approximate analytical shape. The electric current collection is considered over the entire probe. The theory does not consider gas flow, as is the case in the presented here model. It is only valid for electric Reynold's numbers below unity. Sometimes the effect of gas convection around the probe can be significant, as it was demonstrated by other theories [15].

Of course, we only consider the theory for ion saturation current, as the electron saturation current is usually too difficult for use in practice. This probe theory only satisfies plasmas with Maxwellian electron energy distribution and it uses the Einstein relation for the electron and ion diffusion coefficients. Thus, different results are expected both for ion and electron currents if we use a non-Maxwellian EEDF.

$$I_{is} = n_e \left[\frac{2\pi L k (T_e + T_i) \mu_i}{ln\left(\frac{\pi L}{4r}\right)} \right] \tag{8}$$

The expression (8) is formula 2.3 taken from [13], considering the current-voltage characteristic over a finite cylinder (ellipsoid). In the formula, I_{is} is the ion saturation current, n_e is the plasma electron density, L is the electric probe length, r is the probe radius, k is the Boltzmann constant, T_e is the electron temperature in Kelvins, T_i is the ion temperature in Kelvins, and μ_i is the ion mobility.

4. Results and discussion

4.1. Debye sheath and I-V characteristic

The Debye sheath at the probe boundary is evaluated by comparing the electron and ion density. Normally, Debye sheaths would form on boundary areas in plasmas, due to the significant difference in thermal velocity and weight for ions and electrons. Normally, this sheath would be several Debye lengths thick. Figure 4 presents the sheath structure for the conditions noted in the figure caption. Plasma densities in the other figures apply only for the areas of unperturbed plasma.

The model was tested at several plasma densities and electron temperatures. The current-voltage characteristic (figure 5) of the plasma probe of the model is within the expected values, showing the characteristic properties described in plasma probe theory such as plasma potential "knee" and electron saturation current. The electron density n_e noted in the figure caption is the electron density in the unperturbed plasma.
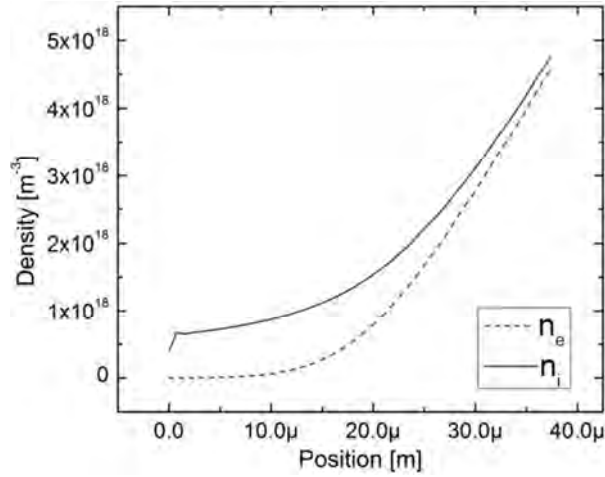
Figure 4. Electron and ion density over distance from probe boundary, at floating potential, $n_{ec} = 1 \times 10^{19} m^{-3}$, $n_e = 1.98 \times 10^{20} m^{-3}$, $T_e = 1$ eV, Maxwellian EEDF.
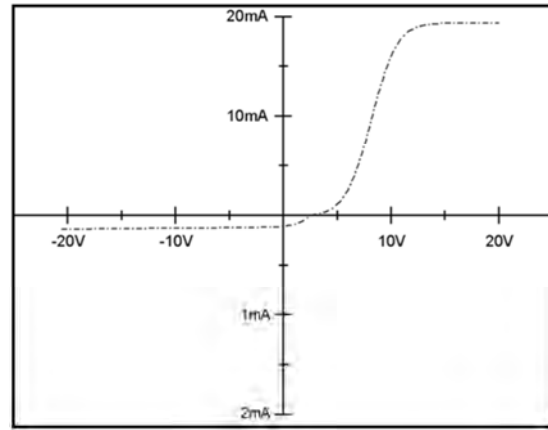

Figure 5. I-V characteristic derived from the model at the following parameters: $n_e = 4.5 \times 10^{19} m^{-3}$, $T_e = 1$ eV and $n_{ec} = 1 \times 10^{19} m^{-3}$, Maxwellian EEDF. Note the different scale for the probe current axis below the zero point.

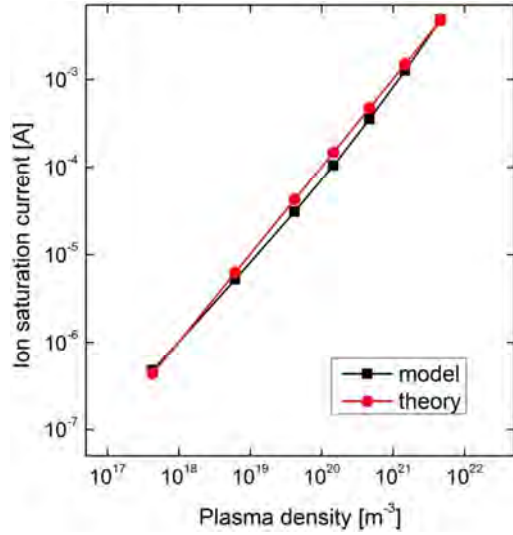### 4.2. Ion saturation current at different electron temperatures

The model is computed iteratively for different plasma densities and electron temperatures. At each completed computation, the values for the ion saturation current are taken at -20V of probe voltage, away from the floating potential, which is usually around 3-5V. For the same density values (figures 6, 7, 8) the ion saturation current is calculated based on the theoretical formula from section 3.
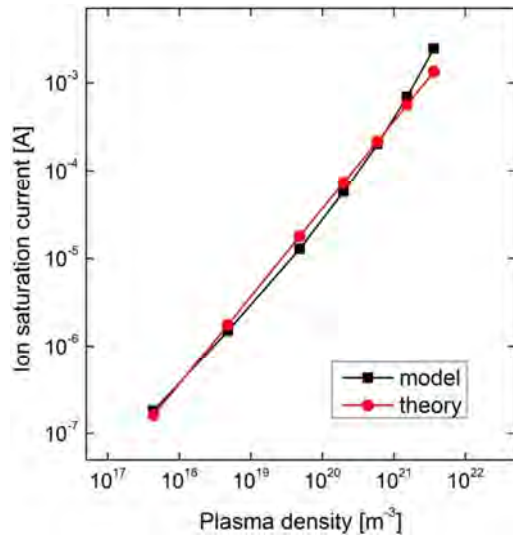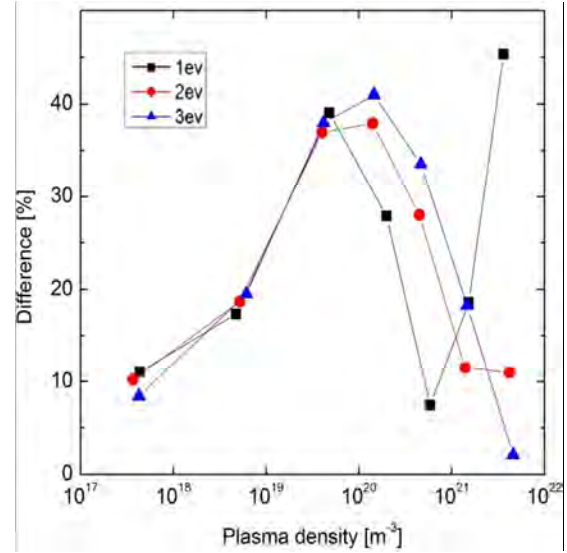

Figure 6. Ion saturation current at different plasma densities, $T_e = 1$ eV, Maxwellian EEDF.
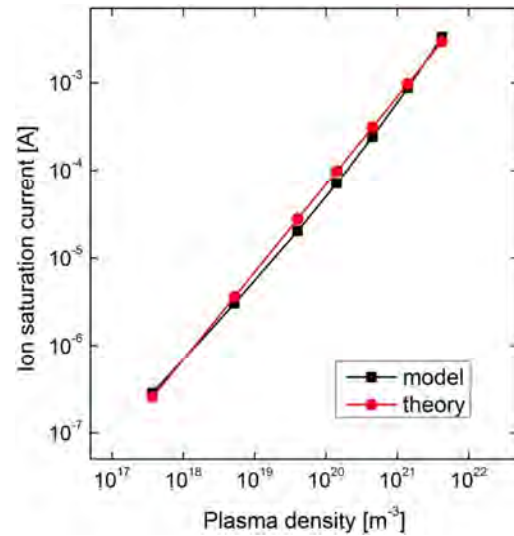
Figure 7. Ion saturation current at different plasma densities, $T_e = 2$ eV, Maxwellian EEDF.

Figure 8. Ion saturation current at different plasma densities, $T_e = 3$ eV, Maxwellian EEDF.

Figure 9. Deviation (in %) of the obtained plasma density based on the analytical model (eq. 8) over the present computational model.

Figure 9 summarizes the results presented in detail in figures 6, 7 and 8. A repetitive trend can be observed between the 3 different settings for electron temperature. At low plasma densities, around 10^{18} and 10^{19} m^{-3}, a very good agreement between the model and the theory is present, with a difference of less than 20%. Further into higher densities, the accuracy worsens reaching 40%. This might be due to the high plasma density and resulting thin sheath areas. However, the behaviour is clearly not linear (figure 9), and other factors such as computational solvers, species density artefacts and time stepping settings can contribute to the total model accuracy. Improving mesh quality (by a factor of 2) at the boundary areas gives little to no benefit. At very high plasma density, we see a difference ranging from 2% to 50%, which is probably due to the geometric approximations of the theory. The expression given by Su and Kiel considers a long ellipsoid, which can only resemble, but not fully describe the cylindrical probe. In the model, we use a cylinder with rounded top (see figure 2). The shape of the probe directly affects the electric field surrounding it, yielding different electron and ion current collection. Overall, the analytical theory by Su and Kiel (8) demonstrates a satisfactory agreement with the results obtained from the computational model. Generally, its deviation is less at lower plasma densities (figure 9).
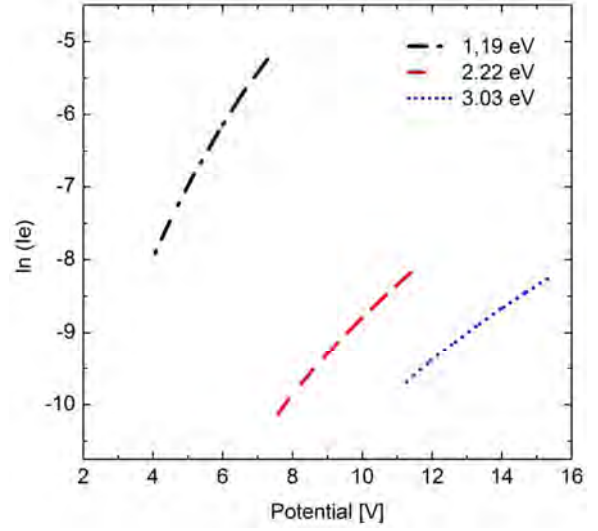
4.3 Derivation of the electron temperature from the electron retardation current
In practice, when using electric probes, usually the electron temperature is unknown and it is derived from the slope of the natural logarithms of the electron retardation current plotted as a function of the probe voltage (at low pressure one could also derive the EEDF and to integrate it in order to obtain the average electron energy). Here we test this approach by deriving T_e from the numerically obtained probe characteristics with known electron temperature of the undisturbed plasma.

In figure 10, the logarithm of the electron current (I_e) is plotted, and part of these curves (figure 11) are used for the derivation of T_e (the obtained values noted in the legend) from their slope. The correspondence with the input values (1, 2 and 3 eV) is very good, compared to the obtained value 1.19 eV, 2.22 eV and 3.03 eV respectively.
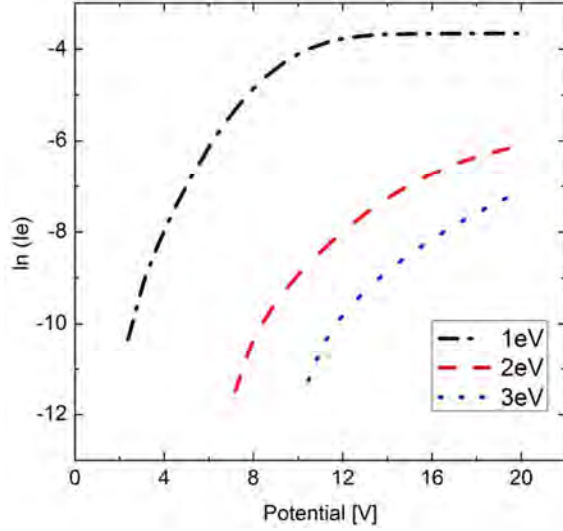
Figure 10. Natural logarithm of electron retardation. Graphs for 1, 2 and 3 eV are shown, for Maxwellian EEDFs. The corresponding electron densities in the simulations are $n_e = 1.99 \times 10^{20}$ m^{-3} ($T_e = 1$ eV), $n_e = 4.02 \times 10^{19}$ m^{-3} ($T_e = 2$ eV), $n_e = 4.15 \times 10^{19}$ m^{-3} ($T_e = 3$ eV)

Figure 11. Parts of the curves shown in figure 12, used for the derivation of the electron temperature.
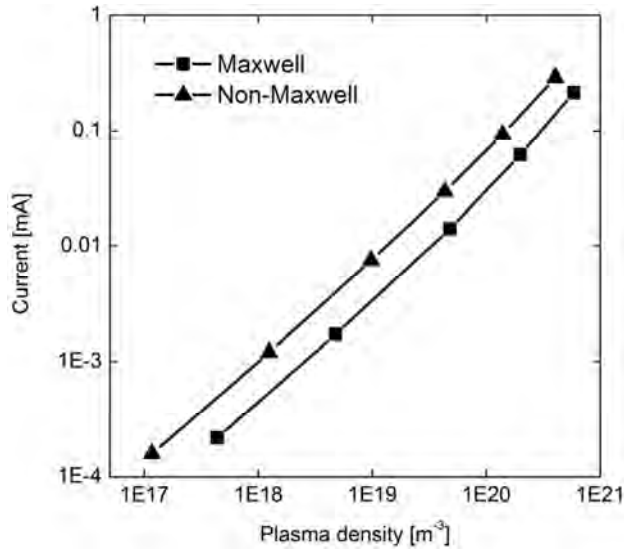
4.4 Ion saturation current at different EEDFs

In this subsection, we show numerical results derived with different EEDFs – Maxwellian and non-Maxwellian (obtained with Bolsig+). Apart from the EEDF itself, the model with a Maxwellian distribution uses the Einstein relation between the electron mobility and diffusion coefficient, while the non-Maxwellian model relies on the electron diffusion coefficients obtained directly from Bolsig+. As a result, in figure 12, a pronounced deviation of the ion saturation current at different plasma densities can be seen. There is a strong deviation in the electron saturation region as well (fig. 13), of over 200%. The plasma potential also changes significantly from 13 V at Maxwellian (Max) EEDF to 31 V for the non-Maxwellian (non-Max) case. This can be explained by a number of factors. In the non-Max models, the electron transport properties differ, i.e. the electron diffusion coefficient is slightly lower (3.58 for non-Max vs 4.39 m^2/s for the Max), but the electron mobility differs significantly (1.40 for non-Max vs 4.39 m^2/V.s for Max). The ion transport properties remain the same (diffusion: 1.22×10^{-4} m^2/s, mobility specification: 8.88×10^{-4} m^2/V.s). The increase of the plasma potential for the non-Max case could be related with increase of the ambipolar electric field, which can be expressed approximately as [31]:

$$E_{amb} \sim \frac{D_e}{\mu_e} \frac{\nabla n_e}{n_e} \qquad (9)$$

At non-Max EEDF the ratio D_e/μ_e increases significantly (2.56 times) which results in increase of the plasma potential in the domain which is around 2.4 times (=31V/13V). The electron saturation current is directly determined by the electron mobility, as it can be seen by equation 2.4 in [13].

With respect to the ion saturation current, the picture is a bit more complicated. According to eq. (8), in the limit of low ion temperature, the ion saturation current is proportional to $\mu_i T_e$. One can speculate that this can be considered as an approximation (assuming low ion diffusivity) of the ambipolar diffusion coefficient ([31], page 136). The ambipolar diffusion (D_a) coefficient increases in the non-Max model : D_a (Max) = 1.01×10^{-3}, while D_a (non-Max) = 2.39×10^{-3}. The above increase of 2.39 times corresponds very well to the increase of the ion saturation current in the non-Max case -

2.3 times. It is also worth noting that it has been shown in the literature that the ion saturation current and the ambipolar potential in low pressure plasmas with non-Maxwellian EEDF are defined by an effective electron temperature which is called electron screening temperature T_{es}. It is determined mainly by the low energy part of the EEDF [32, 33] and it could be approximately derived by the ratio D_e/μ_e [34]. This effective (screening) temperature actually replaces T_e in eq. (8) and since in our case it considerably higher (around 2.3 eV) it determines the ion saturation increase with respect to the Maxwellian case. The above discussion and conclusions, however, include some speculative elements and they can be confirmed only after thorough analytical and numerical analysis, which will be done in a future contribution.

Figure 12. Ion saturation current at different densities, Maxwellian and non-Maxwellian EEDFs, $T_e = 1\text{eV}$, probe voltage -20V.
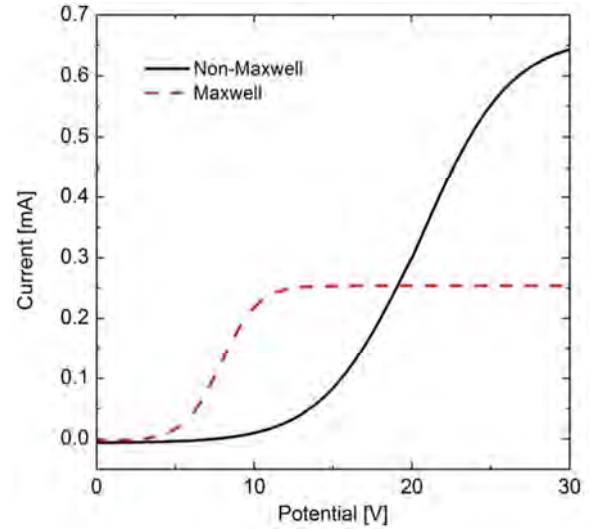
Figure 13. Results for electron current at retarding and saturation regions of I-V characteristic. Parameters: $n_e = 9.7\text{x}10^{18}$ m^{-3}, $T_e = 1$ eV

The later discussion shows also that the ion saturation current is determined primarily by the transport characteristics, and the ionization in the probe sheath is negligible. Indeed, this is confirmed by the examination of the charged particle production in the sheath, which was found to be very small, compared to the particle fluxes from the undisturbed plasma. It is also worth mentioning that numerical tests shows that if we change the electron mobility and diffusion coefficient in both models to the values from the other model, we obtain the ion saturation current, corresponding to the values of the other model from which μ_e and D_e has been taken i.e. if we change μ_e and D_e in the Max model to μ_e and De from non-Max, we obtain ion saturation current equal to the non-Max model, and vice versa, for the non-Max model.

5. Conclusion

The current-voltage characteristic of the simulated probe shows the typical behavior of a probe for the considered conditions. For plasma with a Maxwellian EEDF, the agreement between the probe theory derived in [13] and the numerical model is very reasonable. This is not surprising, as the model uses the drift-diffusion approximation, and the ionisation seems to play a minor role in the probe sheath.

The effect of the probe geometry can lead to a significant difference between the methods, as the computational model uses a thin cylinder, opposed to the ellipsoid approximation used in the analytical model [13]. Thus, a different distribution of the electric field can be expected, resulting in

difference in the probe current. This effect can be seen in the numerical model, where the electric field magnitude has a peak at the probe tip, with twice higher value than the rest of its surface. Moreover, the total probe surface can slightly differ between the analytical expression and the geometry in the model. The trends show that the analytical theory is between 10% and 50% away from the numerical model, which is acceptable for most practical situations. The accuracy of actual low-temperature plasma measurements rarely exceeds this margin. Overall, the numerical model presented here is very versatile, as it covers six magnitudes of plasma density and electron temperatures between 1 and 3 eV, with the possibility for further extension.

The influence of the EEDF on the results is examined. In the given range of plasma densities, the ion saturation current is affected by the particular non-Maxwellian EEDF, showing higher values (figure 12). For the considered conditions of argon gas and gas pressure (atmospheric), using a non-Maxwellian EEDF largely changes the electron mobility coefficient, which leads to a significant difference in the final results. This confirms that the theory [13] is only applicable for a limited range of conditions favouring a Maxwellian energy distribution. Moreover, numerical tests show that since the ionisation processes in the probe sheath play minor role, if one uses the correct values of the transport properties (mobility and diff. coeff.), regardless of the EEDF, the analytical expressions are still reliable enough, although we cannot claim that this is true in general since this was verified only for limited range of conditions and further analysis is needed. The ion saturation current and the ambipolar potential seems to be defined by an effective electron temperature which replaces the electron temperature in eq. (8).

There is a very pronounced deviation in the electron current saturation region as well. Analogically, this is probably related to the different electron mobility.

The comparison of the input electron temperature and the obtained value from the probe is a valuable addition (figure 11), showing a good agreement between model inputs and computational results.

The simplifications taken on the plasma chemical composition are not to be neglected. In high pressure argon discharges, additional species like molecular ions may play a considerable role. Thus, they should be accounted for if more accurate derivation of the ion density is required. In this work, this was omitted in order to provide a more consistent comparison with the analytical expression (8). This is another point of interest for the model accuracy, which is outside the scope of this work.

The gas flow and probe thermal balance are not considered in the model, which might be a strong simplification. In most experiments, the plasma is produced in a flowing gas. The convection of the gas around the probe, depending on the electric Reynolds number, might cause a significant perturbation in the results [15]. The probe thermal balance may influence the plasma in a way of cooling the plasma around it, affecting species mobility and density [1]. However, at this stage, such considerations would complicate the model beyond usability.

As for computational performance, on a workstation equipped with an i7-3820 CPU (4 cores at 3.7GHz) and 64GB of RAM, the model computes within 60 minutes. Of course, numerous iterations are needed for accurate fitting with experimental data.

References

[1] P R Smy, The use of Langmuir probes in the study of high pressure plasmas, *Advances in Physics*, **25**, Issue 5, 517-553, 1976
[2] J Caneses and B Blackwell, RF compensation of double Langmuir probes: modelling and experiment, *Plasma Sources Sci. Technol.*, **24,** 035024, 2015
[3] H M Mott-Smith and I Langmuir, The Theory of Collectors in Gaseous Discharges, *Phys. Rev.*, **28**, 727, 1926

[4] J D Swift and M J R Schwar, *Electrical Probes for Plasma Diagnostics*, London: Iliffe Books, 1970

[5] D Trunec, Z Bonaventura, P Zikin and J Jánský, PIC/MMC Simulation of Electron and Ion Currents to Spherical Langmuir Probe, *Contrib. Plasma Phys.*, **55**, 481-493, 2015

[6] D Yordanov, St Lishev and A Shivarova, How does a probe inserted into discharge influence the plasma structure?, *J. Appl. Physics*, **118**, 183302, 2016

[7] P Chung, L Talbot, K J Touryan, *Electrical probes in stationary and flowing plasmas*, Springer-Verlag, Berlin, Heidelberg, New York, 1975

[8] N Braithwaite and R Franklin, Reflections on electrical probes, *Plasma Sources Sci. Technol.*, **18,** 014008, 2009

[9] C H Su, S H Lam, Continuum Theory of Spherical Electrostatic Probes, *Phys. Fluids*, **6**, 1479, 1963

[10] L M Blair and Kunning G Xu, Langmuir Probe Diagnostics of an Atmospheric-Pressure Microplasma, *AIAA Aviation*, 46th AIAA Plasmadynamics and Lasers Conference

[11] M Benilov, Ion saturation currents to spherical and cylindrical electrostatic probes in collisional plasmas, *J. Appl. Phys.*, **70**, 6726, 1991

[12] R M Clements and P R Smy, The positively biased planar Langmuir probe in a high-pressure plasma, *J. Phys. D: Appl. Phys.*, **26**, 1916-1920, 1993

[13] C H Su and R E Kiel, Continuum Theory of Electrostatic Probes, *J. Appl. Physics*, **37**, 4907, 1966

[14] M S Benilov, Ion saturation currents to spherical and cylindrical electrostatic probes in collisional plasmas, *J. Appl. Phys.*, **70**, 6726, 1991

[15] R M Clemens and P R Smy, Ion Current from a Collision-Dominated Flowing Plasma to a Cylindrical Electrode Surrounded by a Thin Sheath, *J. Appl. Phys.*, **41**, 1970

[16] M S Benilov, Can the temperature of electrons in a high-pressure plasma be determined by means of an electrostatic probe?, *J. Phys. D: Appl. Phys.*, **33**, 1683–1696, 2000

[17] Zh Kiss'ovski , A Ivanov, St Kolev, Plasma parameters of a small microwave discharge at atmospheric pressure obtained by probe diagnostics, *Journal of Physics: Conference* Series, **356**, 012010, 2012

[18] H E Porteanu, S Kühn, R Gesche, Electric probe investigations of microwave generated, atmospheric pressure, plasma jets, *Journal of Applied Physics*, **108**(1), 013301, 2010

[19] Comsol 4.3, *Plasma Module User's Guide*, https://www.comsol.com

[20] Bolsig+, http://www.bolsig.laplace.univ-tlse.fr

[21] E W McDaniel and E A Mason, *The Mobility and Diffusion of Ions in Gases*, Hoboken, NJ: Wiley, 1973

[22] C M Ferreira, J Loureiro and A Ricard, Populations in the metastable and the resonance levels of the argon and stepwise ionization effects in a low-pressure argon positive column, *J. Appl. Phys.*, **57**, 82-90, 1985

[23] BIAGI-v7.1 database, www.lxcat.laplace.univ-tlse.fr; Transcribed from SF Biagi's Fortran code MAGBOLTZ, Version 7.1, 2004, http://consult.cern.ch/writeup/magboltz

[24] K Bartschat and V Zeman, Electron-impact excitation from the (3p54s) metastable states of argon, *Phys. Rev. A*, **59**, 2552, 1999

[25] H A Hyman, Electron-impact ionization cross section for excited states of the rare gases (Ne, Ar, Kr, Xe), cadmium and mercury, *Phys. Rev. A*, **20**, 855-9, 1979

[26] Yu P Raizer, *Gas Discharge Physics*, p 62, Berlin: Springer, 1991

[27] N A Dyadko, Y Z Ionikh, I V Kochetov, D L Marinov, A V Meschanov, A P Napartovich, F B Petrov and S A Starostin, Experimental and theoretical study of the transition between diffuse and contracted forms of the glow discharge in argon, *J. Phys. D: Appl. Phys.*, **41**, 055204, 2008

[28] J Gregório, P Leptrince, C Boisse-Laporteand and L L Alves, Self-consistent modelling of atmospheric micro-plasmas produced by a microwave source, *Plasma Sources Sci. Technol.*, **21**, 015013, 2012

[29] S K Lam, C E Zheng, D Lo, A Dem'yanov and A P Napartovich, Kinetics of Ar_2^* in high-pressure pure argon, *J. Phys. D: Appl. Phys.*, **33**, 242-51, 2000

[30] St Kolev and A Bogaerts, A 2D model for a gliding arc discharge, *Plasma Sources Sci. Technol.*, **24**, 015025, 2015

[31] A Lieberman, A Lichtenberg, *Principles of Plasma Discharges and Materials Processing*, Wiley, DOI: 10.1002/0471724254, 2005

[32] V A Godyak, R B Piejak and B M Alexandrovich, Probe diagnostics of nonMaxwellian plasmas, *J. Appl. Phys.* **73**, 3657, 1993

[33] V A Godyak, R B Piejak and B M Alexandrovich, Electron energy distribution function measurements and plasma parameters in inductively coupled argon plasma, *Plasma Sources Sci. Technol.* **11** 525–543, 2002

[34] J Kim, H Lee, D Kim, Y Kim, Y Kim and C Chung, Investigation of the Boltzmann relation in plasmas with non-Maxwellian electron distribution, *Physics of Plasmas*, **21**, 023511, 2014